NJC

Accepted Manuscript

This is an *Accepted Manuscript*, which has been through the Royal Society of Chemistry peer review process and has been accepted for publication.

Accepted Manuscripts are published online shortly after acceptance, before technical editing, formatting and proof reading. Using this free service, authors can make their results available to the community, in citable form, before we publish the edited article. We will replace this *Accepted Manuscript* with the edited and formatted *Advance Article* as soon as it is available.

You can find more information about *Accepted Manuscripts* in the Information for Authors.

Please note that technical editing may introduce minor changes to the text and/or graphics, which may alter content. The journal's standard Terms & Conditions and the Ethical guidelines still apply. In no event shall the Royal Society of Chemistry be held responsible for any errors or omissions in this *Accepted Manuscript* or any consequences arising from the use of any information it contains.

ROYAL SOCIETY OF CHEMISTRY

www.rsc.org/njc

Ir nanoparticles anchored reduced graphene oxide as a catalyst for oxygen electrode in Li-O_2 cells

Surender Kumar, Selvaraj Chinnathambi, and Nookala Munichandraiah*

Department of Inorganic and Physical Chemistry, Indian Institute of Science, Bangalore – 560012, India

Abstract

Iridium nanoparticles anchored reduced graphene oxide (Ir-RGO) is prepared by simultaneous reduction of graphene oxide and Ir^{3+} ions and its catalytic activity for oxygen electrode in Li-O_2 cells is demonstrated. Ir particles of average size of 3.9 nm are uniformly distributed on the RGO sheets. Oxygen reduction reaction (ORR) is studied on Ir-RGO catalyst in non-aqueous electrolytes by using cyclic voltammetry and rotating disk electrode. Li-O_2 cells with Ir-RGO as the oxygen bifunctional electrode catalyst are subjected to charge-discharge cycling at several current densities. A discharge capacity of 9529 mAh g^{-1} (11.36 mAh cm^{-2}) is obtained initially at a current density of 0.5 mA cm^{-2} (393 mA g^{-1}). There is a decrease in capacity on increasing current density. Although there is a decrease in capacity on repeated discharge-charge cycling initially, a stable capacity is observed for about 30 cycles. The results suggest that Ir-RGO is a useful catalyst for rechargeable Li-O_2 cells.

Key words: Iridium nanoparticles; reduced graphene oxide; bifunctional catalyst; Li-O_2 rechargeable cells; high discharge capacity; cyclability.

---

*Author for correspondence: muni@ipc.iisc.ernet.in

New Journal of Chemistry Accepted Manuscript

Introduction

Oxygen reduction reaction (ORR) is investigated extensively for electrochemical energy storage applications.[1] In proton-exchange membrane fuel cells, O_2 supplied to the cathode undergoes reduction.[2] In metal-air batteries, O_2 present in the atmosphere undergoes reduction at the cathode.[3] As the atmosphere is a rich source of O_2, it is used free of cost in air-breathing mode in these battery systems. In recent years, there is a surge of interest on ORR in non-aqueous media also for Li-air batteries.[4]

Li-air (or Li-O_2) battery has a high theoretical specific energy (11.68 kWh kg^{-1}), which is expected to be a clean and environmental friendly energy source as an alternate to gasoline for vehicular traction.[5] The cell consists of Li metal as the anode and a porous carbon-based oxygen electrode as the cathode in a suitable non-aqueous electrolyte. Among the several scientific and technical problems related to Li-O_2 cell system, studies on rechargeable O_2 electrode with fast kinetics of ORR during the cell discharge and oxygen evolution reaction (OER) during charge in non-aqueous electrolytes are important. In non-aqueous electrolytes, the 1-electron reduction of O_2 to form superoxide (O_2^-) is known to occur as the first step. Subsequently, superoxide undergoes reduction to peroxide (O_2^{2-}) and then to oxide (O^{2-}).[6]

The kinetics of ORR is slow in non-aqueous electrolytes.[1] Furthermore, the reaction needs to be reversible for rechargeable Li-air batteries. In order to realize fast kinetics, a suitable catalyst is essential. The catalyst should be bifunctional for both of ORR and OER in rechargeable battery applications.

Noble metal particles, in particular Pt-based materials, have been extensively investigated as catalyst for ORR in fuel cell.[7] Investigations on Ir-based electrocatalyst are relatively less.

New Journal of Chemistry Accepted Manuscript

Reports on addition of small quantity of Ir to another noble metal such as Pt have gained interest as Ir enhances the catalytic activity and stability.[8-10] The inclusion of Ir in Pt at 5 - 20 wt % Ir was shown to enhance electrocatalytic activity by a factor of more than 1.5. Iridium-based binary and ternary oxide catalysts for both ORR and OER in acidic electrolytes were reported recently.[11] Among the various compositions studied, the Pt-Ir (mass ratio 85:15) catalyst exhibited the highest specific catalytic activity. The effect of Ir on electrocatalytic activity of Pd_3Co alloy was studied theoretically using density functional theory.[12] There was a substantial reduction in the activation barriers of O/OH hydrogenation reactions on introduction of Ir into Pd_3Co, while the O-O scission barrier increased only slightly. The alloying effect attributed to the synergetic interplay between the surface electronic structure modification due to Ir atoms and compressive strain caused by Pd_3Co substrate. Morphology dependent catalytic activity of Ir particles on ORR in acidic and alkaline electrolytes was reported.[13]

Graphene has two-dimensional planar structure with sp^2 bonded carbon atoms. It has become an important electrode material owing to its high electronic conductivity and large surface area.[14] It has been investigated for applications such as supercapacitors, Li-ion batteries, and fuel cells.[15-17] Catalyst nanoparticles prepared and anchored to graphene sheets are expected to sustain discrete existence without undergoing agglomeration and therefore they possess a high catalytic stability for long term experiments as well as applications. In this content, it is intended to explore the catalytic activity of Ir nanoparticles dispersed on reduced graphene oxide (RGO) for ORR. To the best of authors' knowledge, there are no reports on studies of catalytic behaviour of Ir dispersed on RGO towards bifunctional O_2 electrode in non-aqueous electrolyte for Li-O_2 cells.

New Journal of Chemistry Accepted Manuscript

In the present work, Ir nanoparticles deposited on RGO sheets (Ir-RGO) is prepared by in-situ reduction of graphene oxide (GO) and Ir^{3+} ions by sodium borohydride as the reducing agent. Nearly spherical Ir particles of average size of 3.9 nm are anchored on RGO sheets. The Ir-RGO is studied as a catalyst for ORR in both aqueous and non-aqueous electrolytes. Li-O_2 cells assembled using Ir-RGO as the catalyst for bifunctional ORR-OER rechargeable electrode deliver a high discharge capacity with a reasonably good charge-discharge cycling stability. The catalytic activity of Ir-RGO for bifunctional ORR - OER in non-aqueous Li-O_2 cells is reported for the first time.

Experimental

Graphite powder (Graphite India), $NaNO_3$, $KMnO_4$, KOH, $NaBH_4$, $IrCl_3$ (all from S. D. Fine Chemicals), NaCl (Qualigens), $LiPF_6$ (Aldrich), poly vinylidene fluoride (PVDF, Aldrich), n-methyl pyrrolidone (NMP, Aldrich), lithium ribbon (Aldrich) and dimethyl sulphoxide (DMSO, Aldrich) were used as received. Tetrabutyl ammonium perchlorate (TBAP) was prepared by the addition of 10 ml 1M H_3PO_4 to 10 ml 1M tetrabutyl ammonium bromide, recrystallized and dried. Double-distilled water was used for all experiments.

For the preparation of Ir-RGO, graphite powder was first converted into graphite oxide (GtO) by the procedure described by Hummers and Offeman.[18] In brief, graphite powder (3.0 g) was added to 69 ml concentrated H_2SO_4 consisting of 1.50 g $NaNO_3$. The mixture was stirred for 1 h at room temperature. The container was cooled in an ice bath and 9.0 g $KMnO_4$ was added slowly while stirring the contents by a magnetic stirrer for about 15 min. The container was removed from the ice bath and allowed to warm up to ambient temperature. Two aliquots of 138 and 420 ml double-distilled water were added slowly and carefully in about 15 min intervals.

New Journal of Chemistry Accepted Manuscript

Then, 7.5 ml of 30 % H_2O_2 was added. The product GtO was separated by centrifugation, washed with warm water and ethanol several times and dried at 50 ^{0}C for 12 h. GtO (400 mg) was transferred into 800 ml of double-distilled water and sonicated for 3 h. GtO was exfoliated to graphene oxide (GO), which was separated, washed and dried. $IrCl_3$ (155 mg) was added to 100 mg GO, which was dispersed in 600 ml double-distilled water, sonicated for 30 min, and then 5 ml of ammonia was added slowly under stirring. Finally, $NaBH_4$ was added as the reducing agent and the container was kept at 80 ^{0}C for 3 h while stirring the contents. The product, Ir-RGO was separated by centrifugation, washed copiously with double-distilled water and ethanol, and dried at 60 ^{0}C for 12 h. RGO was also prepared in a similar procedure in the absence of $IrCl_3$.

For the rotating disc electrode (RDE) studies, 1.8 mg Ir-RGO and 4 µl Nafion (5 wt % solution) were dispersed in 2 ml ethanol by sonication for 30 min. The suspension (200 µl) was transferred onto a glassy carbon (GC) disk electrode of area 0.07 cm^2 (diameter = 3 mm) and the solvent was evaporated in air. The quantity of Ir–RGO composite was 200 µg on the GC electrode (2.8 mg cm^{-2}). For the preparation of O_2 electrodes for Li-O_2 cells, a porous carbon paper (Toray) of 2.0 mm thickness was employed as the current collector. A circular (12 mm diameter) disk was punched out of a sheet of Toray carbon paper. High surface area (1500 cm^2 g^{-1}) carbon powder (Fuzhou Yihuan Carbon, Co., China) and PTFE suspension (Aldrich) were mixed in 7:3 weight ratios. A few drops of water was added to form a dough, which was rolled into a layer. This layer of mass 185 mg was applied on one side of the carbon paper current collector. The Ir-RGO catalyst and PVDF were mixed (weight ratio: 92.5: 7.5) in a mortar, a few drops of NMP were added to form an ink. The ink was coated on the other side of the carbon paper. The mass of catalyst was 1 mg cm^{-2}. The sandwich of diffusion-layer, carbon paper and

New Journal of Chemistry Accepted Manuscript

catalyst-layer was pressed in a die at a pressure of 50 kN for 3 min. The electrode was dried at 100 ^{0}C for 12 h and transferred into an argon filled MBraun glove box model Unilab. Li-O_2 cells were assembled in home-made Swagelok-type PTFE cell containers. The container had provision to close on one side where Li disk anode was placed and the other side open for exposure to oxygen gas from a cylinder. A Li disk used as the anode (12 mm diameter) was punched out of a ribbon (0.3 mm thick) and its surface was scraped with a knife to remove surface layers on both sides of it. Stainless steel current collectors were used to take electrical contacts from the electrodes. The Li disk, a glass mat separator and the air electrode were sandwiched inside the PTFE container and stainless steel electric contacts were inserted and sealed.[19-21] The glass mat was soaked in the electrolyte, which was made of 1.0 M $LiPF_6$ in DMSO, before inserting into the cell. The catalyst-layer of the O_2 electrode was exposed to the electrolyte and the diffusion-layer to oxygen gas.

For sonication purpose, a Misonix ultra sonicator model S4000-010 was used. It was operated with a frequency of 20 kHz and power output of 600 W. Titanium horn (diameter = 12 mm) was dipped in the aqueous phase and sonicated for the required duration. A Remi ultra centrifuge model R-8C was used to separate the solid samples from liquid phase. A Philips 'X'PERT PRO diffractometer with Cu-Kα radiation (λ: 1.5438 Å) as the X-ray source was used for recording powder X-ray diffraction patterns. UV-visible spectra were recorded by using Perkin-Elmer Lambda 35 UV-visible spectrometer. For this purpose, samples were prepared by sonication in double-distilled water for about 10 min and transferred into a quartz cuvette. FT-IR spectra of powder samples were recorded in a 1000 Perkin Elmer FT-IR spectrometer. Microscopy images of the samples were recorded using FEI Tecnai T-20 200 kV transmission electron microscope (TEM). Rotating disk electrode experiments were conducted using Autolab

New Journal of Chemistry Accepted Manuscript

RDE setup and Autolab potentiostat/galvanostat model PGSTAT 30. The speed of RDE was varied in a wide range from 100 to 2400 rpm while sweeping the potential at 10 mV s^{-1} in ORR potential range. The reference electrodes used include Hg/Hg_2O, KOH (1M) in the alkaline electrolyte and a Pt wire pseudo reference electrode in the non-aqueous electrolyte. All potential values are converted into normal hydrogen electrode (NHE) scale and are presented. Charge-discharge cycling of Li-O_2 cells was carried out by using a Bitrode battery cycling equipment in an air-conditioned room at 22±1 ^{0}C.

Results and discussions

***Physicochemical studies*:** Formation of RGO and Ir-RGO from graphite powder was investigated by powder XRD. The XRD pattern of graphite (Fig. 1a(i)) has a strong (002) reflection at 26.5^0, which corresponds to hexagonal graphitic structure. The inter-layer distance obtained from (002) reflection of graphite is 3.38 Å, which is comparable with the reported values.[22] In the pattern of GtO, there is a shift in the (002) reflection to 10.3^0 (Fig. 1a(ii)). This value corresponds to an inter-layer distance of 8.48 Å. The large increase in inter-layer distance is due to expansion of graphite by the presence of oxygen functional groups on both sides of graphene sheets and also due to atomic scale roughness arising from sp^3 bonding in carbon.[23] There is a shift in the (002) reflection of GO (Fig. 1a (iii)) indicating the conversion of GtO to GO. The RGO is characterized by the low intensity, broad (002) reflection (Fig. 1a (iv)). The diffraction peaks become weak or disappear when regular stacking of GO is disturbed.[24] The broad (002) reflection is also attributed to small sheet size (≤ 1 μm) and a short domain order or turbostatic arrangement of RGO stacked sheets.[25] The XRD pattern of Ir-RGO (Fig. 1b) consists of a broad reflection at 24.2^0 corresponding to the (002) plane of RGO.

New Journal of Chemistry Accepted Manuscript

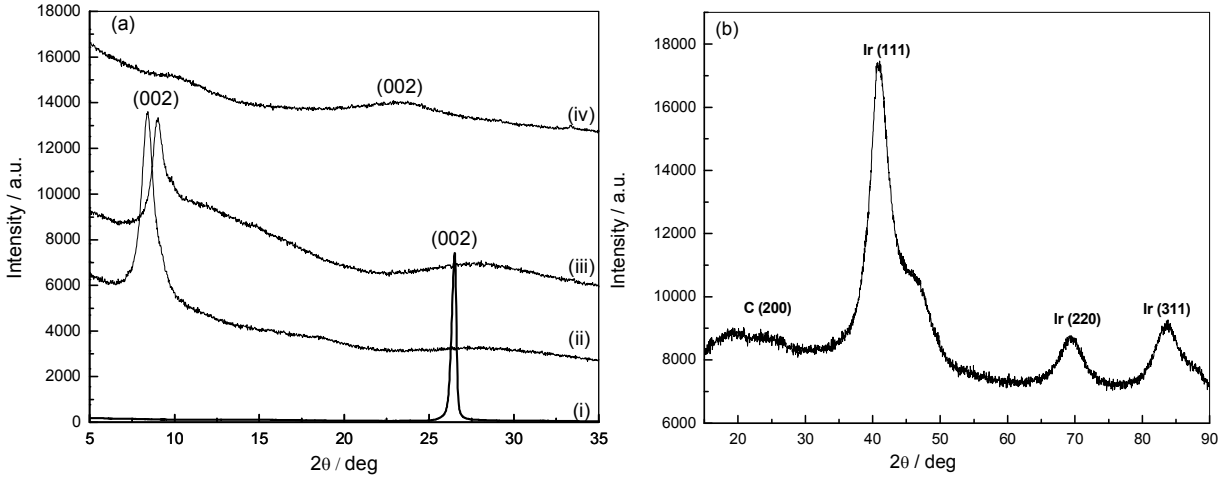

Fig. 1. Powder XRD patterns of (a) graphite (i), graphite oxide (GtO) (ii), graphene oxide (GO) (iii) and reduced graphene oxide (RGO) (iv), and (b) Ir-RGO.

The strong reflections at 40.7, 69.4 and 83.8^0 are assigned to (111), (220) and (311) planes, respectively, of face-centered cubic structure of Ir (JCPDS file 65-1686). Thus, XRD studies (Fig. 1) suggest the conversion of graphite powder to RGO and Ir-RGO.

TEM images of RGO and Ir-RGO are shown in Fig. 2 (a and b). Layers of RGO are seen in Fig. 2a. Nano-sized Ir particles distributed on graphene sheets are seen in the TEM image (Fig. 2b). Ir particles have undergone agglomeration at a few spots. Particle size distribution measured from non-agglomerated particles and plotted in Fig. 2c indicates the presence of Ir nanoparticles in the sizes 3-10 nm, with an average size of 3.9 nm. The distribution of Ir indicates that Ir^{3+} interact with oxygen functionalities in GO. When GO and Ir^{3+} ions are subjected to simultaneous reduction, the interaction facilitates Ir metal nanoparticles to anchor on the surface of RGO sheets. Preparation of Ir-RGO was carried out in a similar procedure and it

New Journal of Chemistry Accepted Manuscript

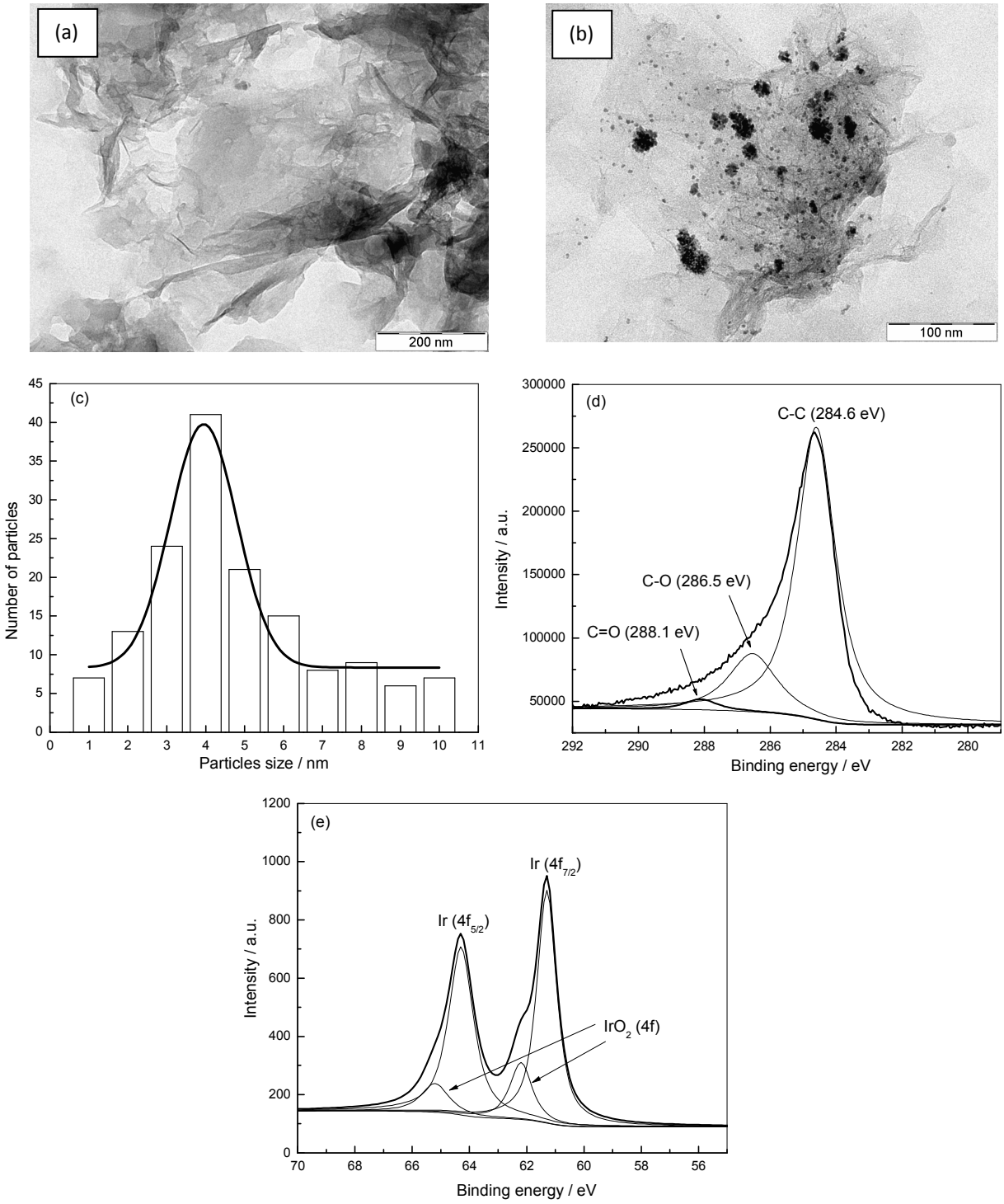

Fig. 2. (a, b) TEM images of RGO and Ir-RGO, (c) particle size distribution of Ir on RGO, and (d, e) XPS spectra of C 1s and Ir 4f orbitals.

New Journal of Chemistry Accepted Manuscript

was investigated as an electrode material for an all – vanadium redox flow battery.[26] Ir nanoparticles of an average size 3 nm were distributed with an occasional agglomeration, similar to the observation made in the present study (Fig. 2b). Ir nanoparticles were considered as spacers, which prevent the restacking of graphitic architecture. The presence of C and Ir in Ir-RGO was also examined by recording XPS spectrum (Fig. 2d and e). The deconvoluted XPS spectrum of C 1s (Fig. 2d) shows the presence of C-C, C-O, and C=O bonds at 284.6, 286.5 and 288.1 eV, respectively. It is known that small quantity of O is present in RGO obtained by the reduction of graphene oxide.[27] Deconvoluted XPS spectrum of Ir-RGO corresponding to 4f core level of Ir (Fig. 2e) consists of a doublet at 61.4 and 64.4 eV. Surface oxidation of Ir results in the formation of a minor quantity of IrO_2.

Electrochemical studies: A Li salt solution is required as the electrolyte for Li-air cell studies. However, such an electrolyte was found unsuitable for RDE studies employing a catalyst coated glassy carbon electrode. Formation of Li_2O and Li_2O_2 occur from the ORR and these

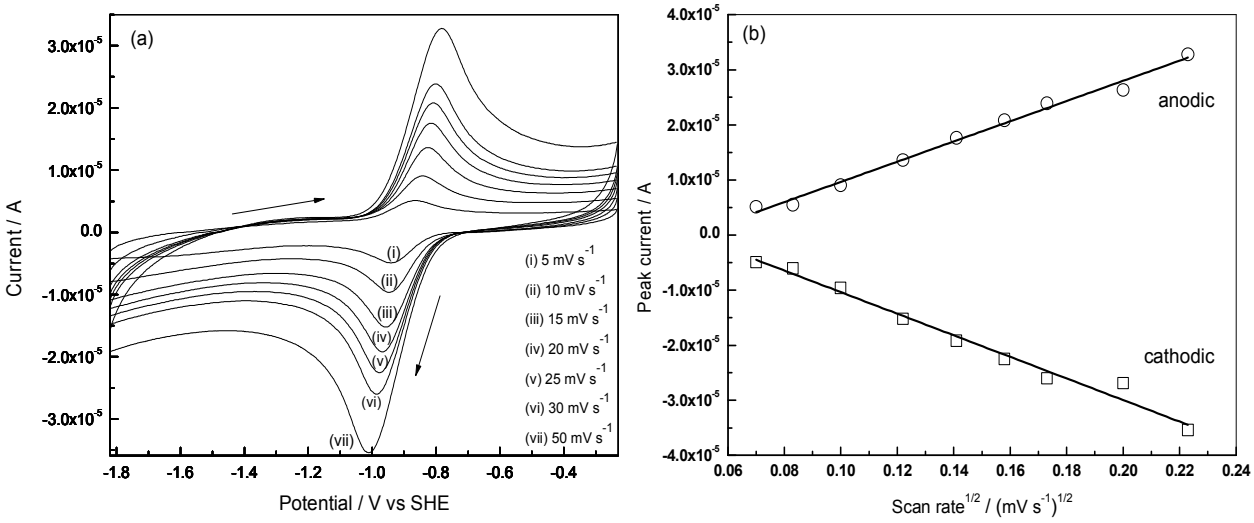

Fig. 3. (a) Cyclic Voltammograms for ORR activity at different scan rates and (b) plot between peak current versus (scan rate)$^{1/2}$ in 0.1M TBAP-DMSO. The area of GC electrode is 0.0314 cm^2 with catalyst mass of 200 µg.

New Journal of Chemistry Accepted Manuscript

oxides deposit on the electrode surface resulting in irreproducibility of experimental results. Therefore, TBAP dissolved in DMSO was used for cyclic voltammetry and RDE studies in the present work, similar to the studies by Laoire et at.[6] Cyclic voltammograms of Ir-RGO coated GC electrode recorded at several sweep rates in 0.1 M TBAP-DMSO electrolyte are shown in Fig. 3a. A cathodic current peak appears at -0.93 V in the forward sweep at 10 mV s^{-1}, which is attributed to the reduction of O_2 resulting in the formation of $TBAO_2$.[6]

$$TBA^+ + O_2 + e^- \longrightarrow TBAO_2 \quad (1)$$

According to the studies reported by Laoire et al,[6] the voltammograms is expected to have another weak current peak. The second cathodic peak was attributed to further reduction of $TBAO_2$ to TBA_2O_2 (reaction 2).

$$TBAO_2 + TBA^+ + e^- \longrightarrow TBA_2O_2 \quad (2)$$

The absence of current peak due to the above step in Fig. 3a is attributed to difference in experimental conditions between the present work and Ref. 6. Thus, the cathodic current peak (P_c) in Fig. 3a. is attributed to the reduction of O_2 (reaction 1) and the anodic peak (P_a) to the opposite reaction. As the anodic charge is nearly equal to the cathodic charge, it is inferred that oxygen reaction is highly reversible in the non-aqueous electrolyte. The cathodic peak current density (i_{pc}) follows Randles – Sevcik equation (Eq. 3).[28]

$$i_{pc} = \left(2.69\, x\, 10^5\right) n^{3/2}\, D^{1/2}\, \nu^{1/2}\, c^o \quad (3)$$

where n is number of electrons, D is diffusion coefficient of O_2, ν is sweep rate and c^o is concentration of O_2 in the electrolyte. A plot of i_{pc} versus $\nu^{1/2}$ is a straight line (Fig. 3b)

New Journal of Chemistry Accepted Manuscript

indicating the ORR is controlled by diffusion of O_2. Similar observation is made for the anodic peak current density (i_{pa}) also from i_{pa} versus $\nu^{1/2}$ data (Fig. 3b).

Linear sweep voltammograms of Ir-RGO coated GC RDE were recorded at a sweep rate of 10 mV s^{-1} with different speeds in 0.1 M TBAP-DMSO solution saturated with O_2 at several speeds (Fig. 4a). At all speeds of the RDE, current is negligibly small between -0.23 and -0.72 V. The reduction current starts increasing at -0.72 V. Current between -0.72 to -1.20 V is due to the mixed control. The steady-state current in the potential range more negative to -1.20 V is due to diffusion controlled ORR. The diffusion–limited steady current density (i_L) is related to the velocity of the RDE by Levich equation.[28]

$$i_L = 0.62\, n\, F\, D^{2/3}\, \eta^{-1/6}\; c^o\; \omega^{1/2} \qquad (4)$$

where η is kinematic viscosity of solution, F is faraday constant and ω (= 2πf) in angular velocity and f is frequency in revolution per second. The data presented in Fig. 4a suggest that the limiting current is a steady value at any speed of RDE. A plot of i_L versus $\omega^{1/2}$ (Fig. 4b) is linear suggesting the validity of Levich equation. Using the value of c^o for O_2 (1.2 x 10^{-6} mol cm^{-3}), and η (0.01 cm^2 s^{-1}), and D of O_2 (1.9 x 10^{-5} cm^2 s^{-1}) in DMSO, the number of electrons involved in oxygen reduction is calculated as 0.85. In the intermediate range of potential (-0.72 to -1.20 V), the reaction is mixed control and Koutesky-Levich equation is valid.

$$\frac{1}{i} = \frac{1}{nFkc^o} + \frac{1.61\,\eta^{1/6}}{nFc^oD^{2/3}}\frac{1}{\omega^{1/2}} \qquad (5)$$

where k is rate constant. A plot of i^{-1} versus $\omega^{-1/2}$ is expected to be linear. Plots of i^{-1} versus $\omega^{-1/2}$ at different potentials in the range from -0.07 to -0.10 V are presented in Fig. 4c. The average

New Journal of Chemistry Accepted Manuscript

value of D calculated from the slopes is 1.82 x 10^{-5} cm^2 s^{-1}, which agrees well with the value reported in the literature.[29]

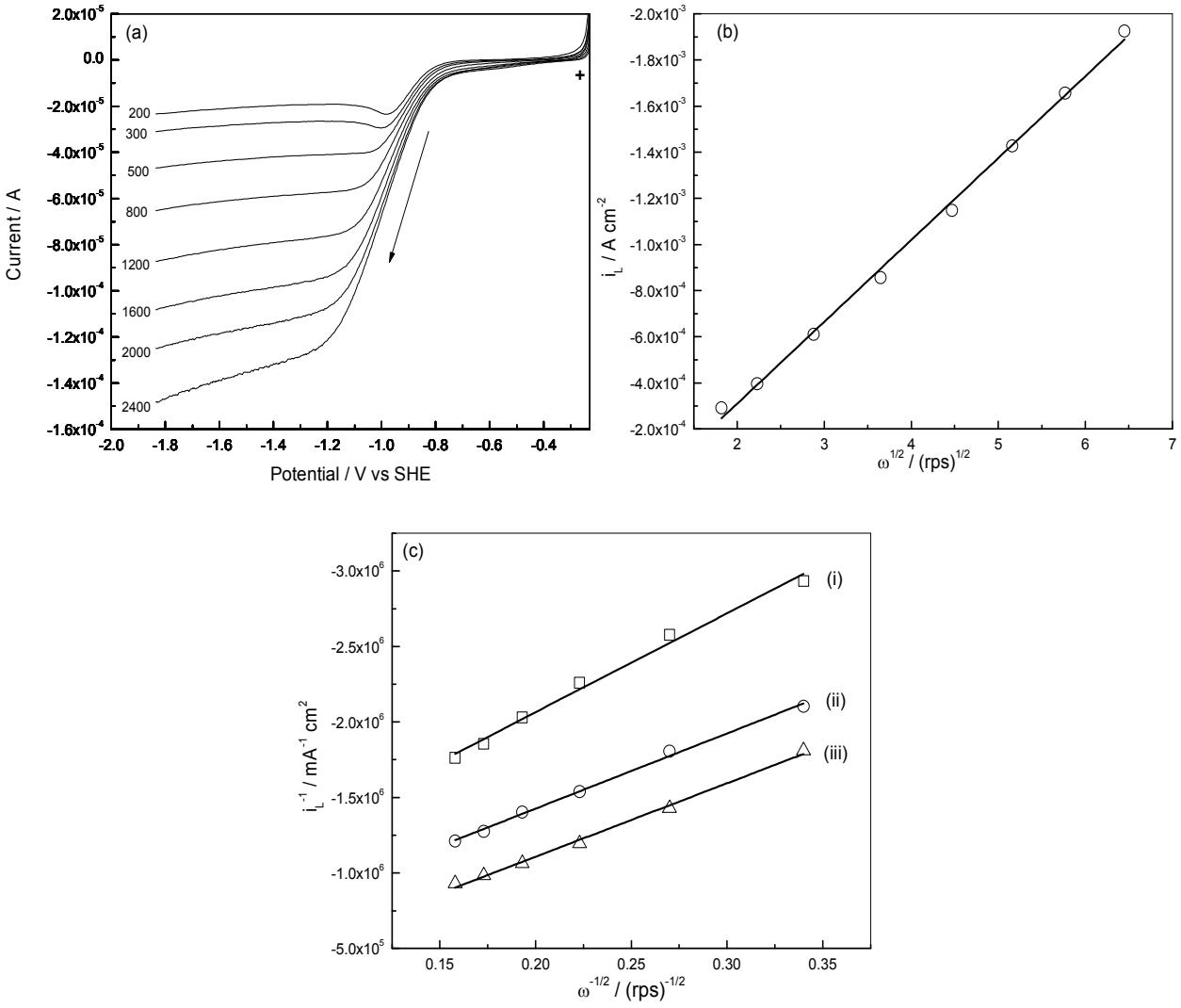

Fig. 4. (a) Linear sweep voltammograms at 10 mV s^{-1} with different speeds (rpm) of rotation in O_2 saturated 0.1M TBAP-DMSO, (b) Levich plot at -1.60 V, and (c) Koutecky-Levich plots at -0.92 (i), -0.97 (ii) and -1.02 V (iii) . The area of GC electrode is 0.0314 cm^2 with catalyst mass of 200 µg.

New Journal of Chemistry Accepted Manuscript

$$O_2 + e^- \longrightarrow O_2^- \quad (6)$$

As the value of n (=0.85) is close to unity, it is inferred that the formation of superoxide (O_2^-) in the non-aqueous electrolyte is the rate determining step (reaction 6).

In order to study the effect of Ir nanoparticles on RGO sheets, RDE experiments were conducted with GC electrode coated with RGO under identical experimental condition. Cyclic voltammograms recorded for RGO and Ir-RGO are compared in Fig. 5a. There are currents peaks corresponding to ORR and OER on RGO similar to the voltammogram of Ir-RGO. However, the current peaks are substantially smaller on RGO in relation to Ir-RGO. The oxidation current peak of RGO is considerably smaller. The ratios of cathodic peak current to the anodic peak current are 0.48 and 1.06 respectively, for RGO and Ir-RGO.

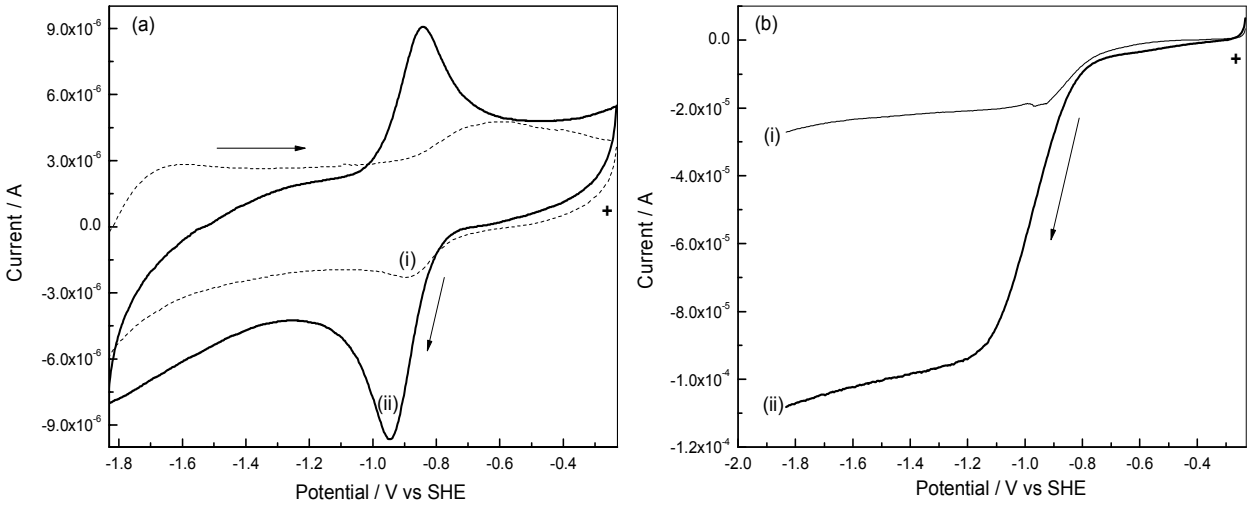

Fig. 5. (a) Cyclic voltammogram at 10 mV s^{-1}, (b) linear sweep voltammograms of RDE at 1600 rpm and 10 mV s^{-1} of RGO (i) and Ir-RGO coated GC electrode in O_2 saturated 0.1 M TBAP-DMSO solution. The area of GC electrode is 0.0314 cm^2 with catalyst mass of 200 µg.

New Journal of Chemistry Accepted Manuscript

Furthermore, linear sweep voltammogram of RGO and Ir-RGO coated GC electrode recorded at 1600 rpm and 10 mV s^{-1} sweep rate are compared in Fig. 5b. The limiting current measured for ORR on Ir-RGO is several times greater than that of on RGO. These results suggest poor catalytic activity of RGO in relation to Ir-RGO. Greater reversibility of ORR-OER is expected on Ir-RGO.

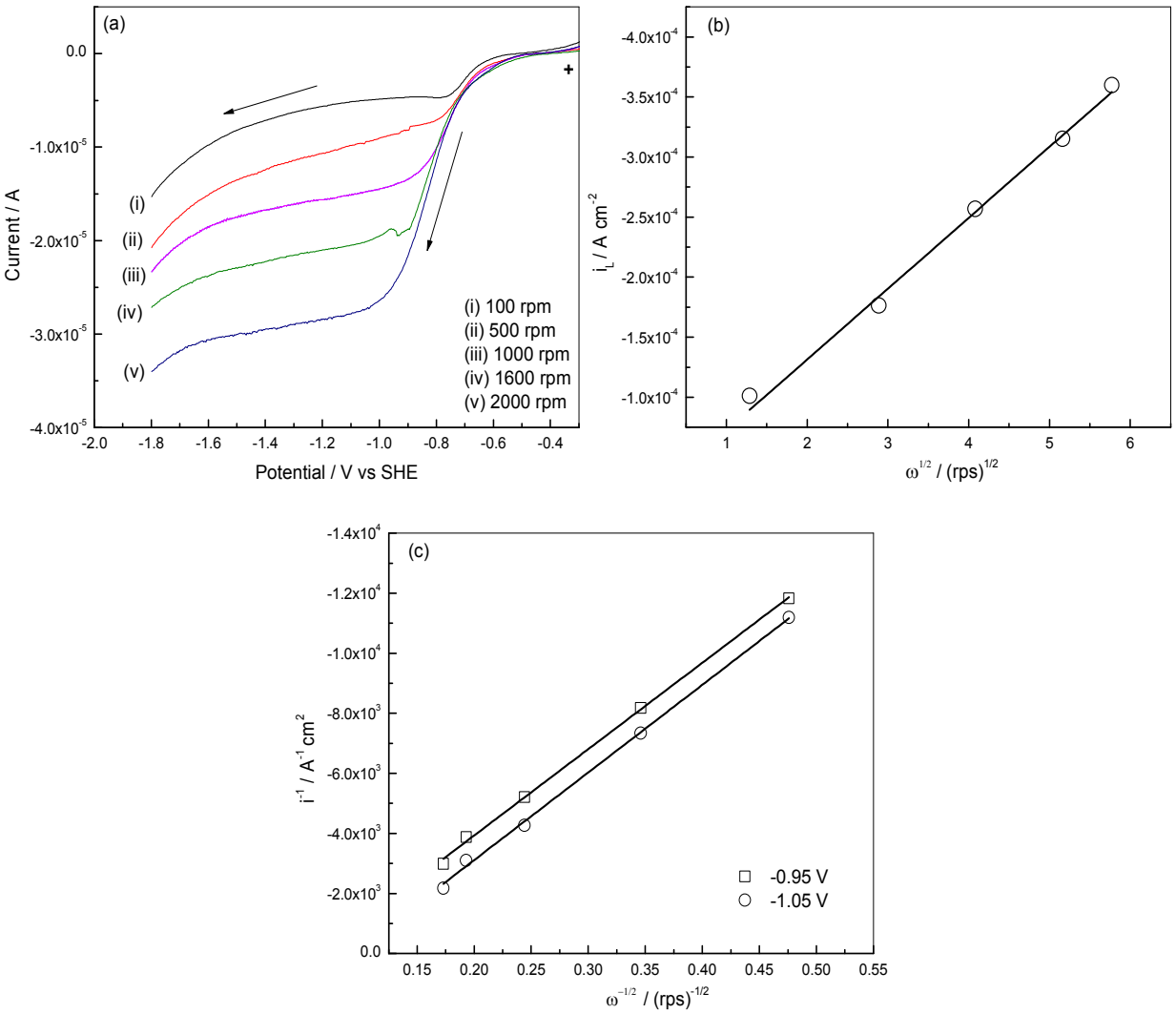

Fig. 6. (a) Linear sweep voltammograms on RGO at 10 mV s^{-1} with different speeds of rotation in O_2 saturated 0.1 M TBAP-DMSO, (b) Levich plot at -1.40 V, and (c) Koutecky-Levich plot at -0.95 and -1.05 V. The area of GC electrode is 0.0314 cm^2 with catalyst mass of 200 µg.

New Journal of Chemistry Accepted Manuscript

Linear sweep voltammograms of RGO coated GC RDE in O_2 saturated 0.1 M TBAP-DMSO solution were also recorded at several speeds (Fig. 6a). The data of RGO follow Levich equation (Fig 6b) and Koutecky-Levich equation (Fig. 6c) similar to the data of Ir-RGO coated GC electrode. The values of D and n obtained for RGO are 1.01 x 10^{-6} cm^2 s^{-1} and 0.46 respectively. These results suggest that the catalytic activity of Ir-RGO for ORR is due to the Ir particles present on RGO sheets.

Li-O_2 cell studies: The electrochemical properties of O_2 electrode of Li-O_2 cells depend on several factors, which include the nature of carbon, catalyst, the current collectors, the electrolyte as well as the electrodes fabrication. In the present work, 1.0 M $LiPF_6$ dissolved in DMSO as the electrolyte and porous Toray carbon paper as the current collecting substrate were used. On a side of the carbon paper, a diffusion-layer made of high surface area (1500 cm^2 g^{-1}) carbon powder with micropores of diameter less than 2 nm was coated with a quantity of 185 mg cm^{-2}.[20] This side was exposed to O_2 gas. The other side of the carbon paper, which was exposed to the electrolyte, was coated with the catalyst. This procedure of fabrication of the air-electrode was optimized after conducting several trial experiments. The Li-air cells did not provide satisfactory discharge capacity, when they were assembled either with bare carbon paper, RGO coated carbon paper or the Ir-RGO catalyst alone coated carbon paper air-electrode. The performance of the cells improved only when the PTFE bonded carbon layer was present on the rear side of the carbon paper, which was exposed to O_2 gas. Several cells were assembled by varying the quantity of carbon and evaluated their discharge behaviour. A maximum capacity was obtained when the loading level of carbon was 185 mg. Hence all cells were assembled using a carbon paper coated with the catalyst on one side and teflonised carbon on the other side. The carbon layer acts as a diffusion layer for O_2 gas. Several cells were assembled and tested for

New Journal of Chemistry Accepted Manuscript

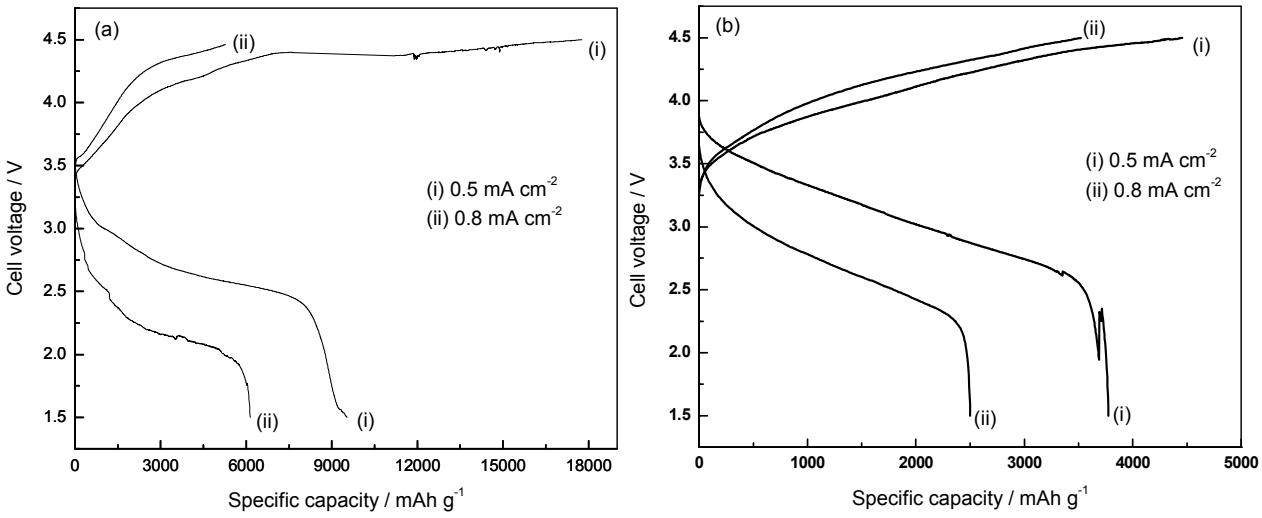

Fig. 7. Discharge-charge voltage profiles of Li-O_2 cell at (a) first discharge followed by first charge, and (b) third charge and fourth discharge at current densities of 0.5 and 0.8 mA cm^{-2}.

Li-air study. The open circuit voltage of the as assembled cells was about 3.50 V. The cells were first discharged to 1.50 V and then charged to 4.50 V. Specific capacity values of the fresh cells was 11449 (12.24), 9529 (11.36), and 6162 mAh g^{-1} (6.73 mAh cm^{-2}), at specific current density of 0.2, 0.5, and 0.8 mA cm^{-2} respectively**.** The voltage profiles of Li-O_2 cells recorded during the first discharge, followed by charge are shown in Fig. 7a. The capacity of the first charge exceeds the capacity obtained in the previous discharge, thus, suggesting the decomposition of the electrolyte. For the purpose of examining the electrolyte decomposition, a Li-O_2 cell was subjected to repeated charge-discharge cycles and the electrolyte was tested by infrared (IR) and nuclear magnetic resonance (NMR) spectroscopy. The IR and NMR spectra of the fresh electrolyte and the used electrolyte were alike, thus indicating the absence of any decomposition products of the electrolyte. Although the first charge capacity was greater than the first discharge capacity (Fig. 7a), it was found that the difference in the capacities of charge and discharge

New Journal of Chemistry Accepted Manuscript

decreased considerably on repeating cycling as observed in the voltage profile of 3rd charge-discharge cycle (Fig. 7b). At 0.5 mA cm^{-2}, the average discharge voltage is about 3.0 V and the charge voltage is about 4.0 V. The voltage difference between charge and discharge curves is more than 1 V. When the current density is increased to 0.8 mA cm^{-2}, there is a decrease in discharge voltage, while charge voltage is increased due to high polarization at the air electrode. The specific capacity of the cell also decreased, as expected**.** A wide range of discharge capacity values are reported in the literature. For instance, discharge capacity of 1400 mAh g^{-1} with cobalt phthalocyanine catalyst,[4] 1000 mAh g^{-1} with electrolytic MnO_2,[30] 3000 mAh g^{-1} with α-MnO_2,[31] 2700 mAh g^{-1} with Fe_2O_3,[32] 225 mAh g^{-1} with Pd-MnO_2,[33] 4750 mAh g^{-1} with MnO_2 catalyst,[34] about 3000 mAh g^{-1} with Vulcan carbon,[35] 5900 mAh g^{-1} with Pd modified carbon,[36] 5000 mAh g^{-1} with RuO_2 –RGO hybrid catalyst,[37] 8706 mAh g^{-1} with graphene,[38] and 15,000 mAh g^{-1} with graphene catalyst[39] are reported for Li-O_2 cells. A comparison of discharge capacity obtained in the present study with the values reported in the literature could be inconclusive because there is no uniformity in experimental conditions such as cell configurations, current collectors, electrodes fabrication, nature of the catalyst and its loading level, electrolytes, current densities used for charge-discharge cycling, etc.

The charge-discharge reactions are as follows.

At the negative electrode:

$$Li^+ + e^- \underset{\text{charge}}{\overset{\text{discharge}}{\rightleftharpoons}} Li \qquad (10)$$

New Journal of Chemistry Accepted Manuscript

It is known that the reduction of O_2 in Li^+ ion containing non-aqueous electrolytes results in the formation of Li_2O_2 and Li_2O as stable products during the discharge of Li-O_2 cell. Laoire *et al*.,[6] proposed the following mechanism for oxygen reduction:

$$O_2 + Li^+ + e^- \underset{\text{charge}}{\overset{\text{discharge}}{\rightleftharpoons}} LiO_2 \quad (11)$$

$$LiO_2 + Li^+ + 2e^- \underset{\text{charge}}{\overset{\text{discharge}}{\rightleftharpoons}} Li_2O_2 \quad (12)$$

$$Li_2O_2 + 2Li^+ + 2e^- \underset{\text{charge}}{\overset{\text{discharge}}{\rightleftharpoons}} 2Li_2O \quad (13)$$

Single-electron transfer reduction of O_2 produces superoxide (O_2^-) in non-aqueous electrolytes (reaction 11). Lithium superoxide undergoes reduction (reaction 12) forming lithium peroxide, which further undergoes two electron transfer reduction (reaction 13) forming the final product, Li_2O. It is also believed that the reaction intermediate formed during oxygen reduction, namely, O^{2-} is reactive towards most of the solvents used for the electrolyte, which may lead to the formation of Li_2CO_3.[40, 41] Although Li_2CO_3 was considered as difficult to decompose during charging,[42] it was later reported that the anodic decomposition of Li_2CO_3 was favourable when a suitable catalyst such as NiO was used.[43, 44] Lithium oxides are expected to be the major reaction products of oxygen reduction in the non-carbonate based electrolytes.[45, 46] In the present study also, Li_2O_2 and Li_2O are identified as the major products of O_2 reduction during the discharge of Li-O_2 cells, as discussed later. During the charging process, Li_2O_2 and Li_2O are converted to O_2 following the reverse steps of reactions 13, 12 and 11 in sequence.

New Journal of Chemistry Accepted Manuscript

Mechanistically, the adsorption of O_2 on the catalyst surface is expected to be the primary step of ORR. In the case of nanoparticles of Ir, which are anchored to RGO surface, it is expected that the Ir particles possess surface defects facilitating adsorption O_2. The adsorbed O_2, thus, undergoes electron-transfer in the presence of Li^+ ions producing LiO_2, Li_2O_2 and Li_2O (reactions 11-13) during discharge of Li-O_2 cells. The reverse reactions occur resulting in OER during the charging process.

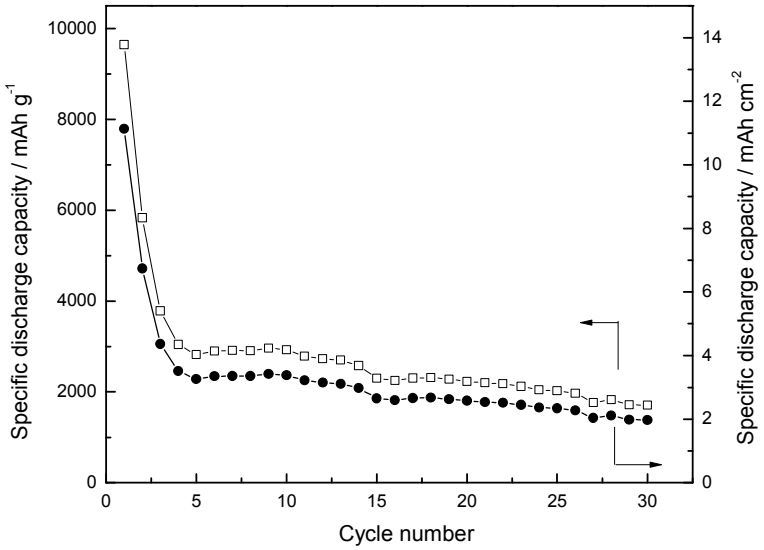

Fig. 8. Cycle life test at current density 0.5 mA cm^{-2}.

Li-O_2 cells were tested for cycling stability at a current density of 0.5 mA cm^{-2} over 30 cycles (Fig. 8). Initially, about 9529 mAh g^{-1} (11.36 mAh cm^{-2}) is obtained. There is a rapid decrease in capacity to 2822 mAh g^{-1} (3.25 mAh cm^{-2}) at 5th Cycle. This was followed by a gradual decrease in capacity. The discharge capacity 1710 mAh g^{-1} (1.97 mAh cm^{-2}) is obtained for the 30^{th} cycle. When Li-O_2 cells were cycled, the discharge capacity decreased rapidly in

New Journal of Chemistry Accepted Manuscript

about 5-10 cycles and the cells could not be cycled thereafter. These results confirm the catalytic activity of Ir-RGO for oxygen electrode reaction in non-aqueous rechargeable Li-O_2 cells. Thus, Ir-RGO is a promising catalyst for rechargeable Li-O_2 cells.

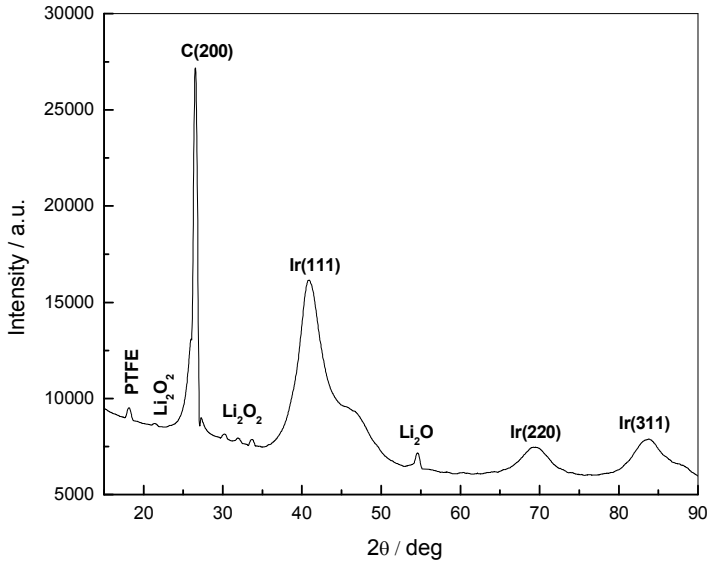

Fig. 9. XRD pattern of oxygen electrode after subjecting a Li–O_2 cell to five charge–discharge cycles.

In order to identify the reaction products of O_2 reduction on Ir-RGO in DMSO electrolyte, a few Li-O_2 cells were assembled, subjected to about ten charge-discharge cycles and terminated the cycling after the cells were discharged. The cells were dissembled, washed with acetone and XRD patterns of the oxygen electrodes were recorded (Fig. 9). The XRD patterns recorded for all electrodes were similar, thus, ensuring the reproducibility of the results. The (002) reflection of carbon is present at 26.7^0. This is the most intense peak of the XRD pattern because of the presence of porous carbon paper current collector, diffusion layer made of carbon powder and also RGO present in Ir-RGO catalyst. The reflections corresponding to (111), (220)

New Journal of Chemistry Accepted Manuscript

and (311) planes of face-centered cubic crystal of Ir appear at 40.7, 69.4 and 83.8^0., respectively. These reflections remain the same as those of the as prepared Ir-RGO catalyst (Fig. 1b). As there are no changes noticed in the crystal structure of Ir after repeated charge-discharge cycling, the stability of the catalyst is ensured. In addition to the reflections of carbon and Ir, there are a few more peaks or shoulders present in the cycled electrode. The reflection at 18.2^0 is attributed to the PTFE binder present in Toray carbon paper, the shoulder at 31.6^0 and peak at 54.7^0 are due to Li_2O, and a weak shoulder at 48^0 is due to Li_2O.[46-48] Thus, Li_2O_2 and Li_2O are inferred as the products of O_2 reduction in the present study.

Conclusion

Iridium nanoparticles anchored reduced graphene oxide is prepared by simultaneous reduction of graphene oxide and Ir^{3+} ions using sodium borohydride as the reducing agent. Ir particles of average size of 3.9 nm are distributed on the RGO sheets. Oxygen reduction reaction is studied on Ir-RGO catalyst in aqueous and non-aqueous electrolytes by using cyclic voltammetry and rotating disk electrode techniques. Li-O_2 cells with Ir-RGO as oxygen electrode catalyst are subjected to charge-discharge cycling at several current densities. A discharge capacity of 9648 mAh g^{-1} is obtained initially at low a current density. There is a decrease in capacity on increasing the current density. Although there is a decrease in capacity on repeated discharge-charge cycling, stable capacity is observed for about 30 cycles tested. The results indicate that Ir-RGO is a suitable catalyst for rechargeable Li-O_2 cells.

New Journal of Chemistry Accepted Manuscript

References

[1] E. Yeager, *J. Mol. Catal.* 1986, **38**, 5-25.

[2] M. K. Debe, *Nature* 2012, **486**, 43-51.

[3] J.-S. Lee, S. T. Kim, R. Cao, N.-S. Choi, M. Liu, K. T. Lee and J. Chao, *Adv. Energy Mater.* 2011, **1**, 34-50.

[4] K. M. Abraham and Z. Jiang, *J. Electrochem. Soc.* 1996, **143**, 1-5.

[5] G. Girishkumar, B. McCloskey, A. C. Luntz, S. Swanson and W. Wilcke, *J. Phys. Chem. Lett.* 2010, **1**, 2193-2203.

[6] C. O. Laoire, S. Mukerjee and K. M. Abraham, *J. Phys. Chem. C.* 2009, **113**, 20127-20137.

[7] Y. Xu, A. V. Ruban and M. Mavrikakis, *J. Am. Chem. Soc.* 2004, **126**, 4717-4725.

[8] T. Ioroi and K. Yasuda, *J. Electrochem. Soc.* 2005, **152**, A1917-A1924.

[9] E. W. Brooman and T. P. Hoar, *Platinum Metal Rev.* 1965, **9**, 122-125.

[10] R. Zhang and W. Chen, *J. Mater. Chem. A* 2013, **1**, 11457–11464.

[11] E. Antolini, *ACS Catal.* 2014, **4**, 1426−1440.

[12] H. C. Ham, D. Manogaran, K. H. Lee, K. Kwon, S.-A. Jin, D. J. You, C. Pak and G. S. Hwang, *J. Chem. Phys.* 2013, **139**, 201104-201107.

[13] K. Chakrapani and S. Sampath, *Phys. Chem. Chem. Phys.* 2014, **16**, 16815-16823.

[14] A. K. Geim and K. S. Novoselov, *Nature Mater.* 2007, **6**, 183-191.

[15] E. Antolini, *Appl. Catal. B: Env.* 2012, **123– 124**, 52– 68.

[16] S. Bose, T. Kuila, A. K. Mishra, R. Rajasekar, N. H. Kim and J. H. Lee, *J. Mater. Chem.* 2012, **22**, 767-784.

[17] M. Liang and L. Zhi, *J. Mater. Chem.* 2009, **19**, 5871–5878.

[18] W. S. H. Jr and R. E. Offeman, *J. Am. Chem. Soc.* 1958, **80**, 1339.

New Journal of Chemistry Accepted Manuscript

[19] M. Eswaran, N. Munichandraiah and L. G. Scanlon, *Electrochem. Solid-State Lett.* 2010, **13,** A121-A124.

[20] S. Kumar, C. Selvaraj, N. Munichandraiah and L. G. Scanlon, *RSC Adv.* 2013, **3**, 21706-21714.

[21] C. Selvaraj, N. Munichandraiah and L. G. Scanlon, *J. Porphyrins Phthalocyanines* 2012, **16**, 255-259.

[22] J. Yang, C. Zhang, L. Sun, N. Zhao and X. Cheng, *Mater. Chem. Phys.* 2011, **129**, 270-274.

[23] J. Shen, Y. Hu, M. Shi, X. Lu, C. Qin and C. Li, *Chem. Mater.* 2009, **21**, 3514-3520.

[24] C. Xu, X. Wang, L. Yang and Y. Wu, *J. Solid State Chem.* 2009, **182**, 2486-2490.

[25] S. Dubin, S. Gilje, K. Wang, V. C. Tung, K. Cha, A. S. Hall, J. Farrar, R. Varshneya, Y. Yang and R. B. Kaner, *ACS Nano* 2010, **4**, 3845-3852.

[26] H.-M. Tsai, S.-J. Yang, C.-C. M. Ma and X. Xie, *Electrochim. Acta* 2012, **77**, 232-236.

[27] S. Pei and H.-M. Cheng, *Carbon* 2012, **50**, 3210 – 3228.

[28] A. J. Bard and L. R. Faulkner, *Electrochemical Methods: Fundamental and Application*, John Wiley and Sons, 1980, p.1.

[29] X. Zhou, Z. Yang, H. Nie, Z. Yao, L. Zhang and S. Huang, *J Power Sources* 2011, **196**, 9970–9974.

[30] T. Ogasawara, A. Debart, M. Holzapfel, P. Novak and P. G. Bruce, *J. Am. Chem. Soc.* 2006, **128**, 1390-1393.

[31] A. Debart, A. J. Paterson, J. Bao and P. G. Bruce, *Angew, Chem. Int. Ed.* 2008, **47**, 4521-4524.

[32] A. Debart, J. Bao, G. Armstrong and P. G. Bruce, *J. Power Sources* 2007, **174**, 1177-1182.

[33] A. K. Thapa, K. Saimen and T. Ishihara, *Electrochem. Solid-State Lett.* 2010, **13**, A165-

New Journal of Chemistry Accepted Manuscript

A167.

[34] H. Cheng and K. Scott, *J. Power Sources* 2010, **195**, 1370-1374.

[35] Y.-C. Lu, D. G. Kwabi, K. P. C. Yao, J. R. Harding, J. Zhou, L. Zuind and Y. Shao-Horn, *Energy Environ. Sci.* 2011, **4**, 2999–3007.

[36] J.-J. Xu, Z.-L. Wang, D. Xu, L.-L. Zhang and X.-B. Zhang, *Nat. Commun.* 2013, **4**, 1-10.

[37] H.-G. Jung, Y. S. Jeong, J.-B. Park, Y.-K. Sun, B. Scrosati and Y. J. Lee, *ACS Nano* 2013, **7**, 3532–3539.

[38] Y. Li, J. Wang, X. Li, D. Geng, R. Li and X. Sun, *Chem. Commun.* 2011, **47**, 9438–9440.

[39] J. Xiao, D. Mei, X. Li, W. Xu, D. Wang, G. L. Graff, W. D. Bennett, Z. Nie, L. V. Saraf, I. A. Aksay, J. Liu and J.-G. Zhang, *Nano Lett.* 2011, **11**, 5071–5078.

[40] D. Xu, Z. Wang, J. Xu, L. Zhang and X. Zhang, *Chem. Comm.* 2012, **48**, 6948 – 6950.

[41] S. A. Freunberge, Y. Chen, Z. Pneg, J. M. Griffin, L. J. Hard-wick, F. Bard, P. Novak and P. G. Bruce, *J. Am. Chem. Soc.* 2011, **133**, 8040-8047.

[42] K. Takechi, T. Shiga and T. Asaoka, *Chem. Commun.* 2011, **47**, 3463–3465.

[43] R. Wang, X. Yu, J. Bai, H. Li, X. Huang, L. Chen and X. Yang, *J. Power Sources* 2012, **218**, 113-118.

[44] Y. Liu, R. Wang, Y. Lyu, H. Li and L. Chen, *Energy Environ. Sci.* 2014, **7**, 677–681.

[45] S. A. Freunberger, Y. Chen, N. E. Drewett, L. J. Hardwick, F. Barde and P. G. Bruce, *Angew. Chem. Int. Ed.* 2011, **50**, 8609-8613.

[46] D. Sharon, V. Etacheri, A. Garsuch, M. Afri, A. A. Frimer and D. Aurbach, *J. Phys. Chem. Lett.* 2013, **4**, 127-131.

New Journal of Chemistry Accepted Manuscript